Evaluation of a Convective Downburst Prediction Application for India

Kenneth L. Pryor*
National Oceanic and Atmospheric Administration (United States)/Center for Satellite Applications and Research, 5830 University Research Court, College Park, MD 20740
C. J. Johny, V. S. Prasad
National Center for Medium Range Weather Forecasting, A-50, Sector 62, Noida, UP, India

ABSTRACT

During the month of June 2015, the South Asian (or Southwest) monsoon advanced steadily from the southern to the northwestern states of India. The progression of the monsoon had an apparent effect on the relative strength of convective storm downbursts that occurred during June and July 2015. A convective downburst prediction algorithm, involving the Microburst Windspeed Potential Index (MWPI) and a satellite-derived three-band microburst risk product, and applied with meteorological geostationary satellite (KALPANA-1 VHRR and METEOSAT-7) and Aqua MODIS data, was evaluated and found to effectively indicate relative downburst intensity in both pre-monsoon and monsoon environments over various regions of India. The MWPI product, derived from T574L64 Global Forecast System (NGFS) model data, is being generated in real-time by National Center for Medium Range Weather Forecasting (NCMRWF), Ministry of Earth Sciences, India. The validation process entailed direct comparison of measured downburst-related wind gusts at airports and India Meteorological Department (IMD) observatories to adjacent MWPI values calculated from GFS and India NGFS model datasets. Favorable results include a statistically significant positive correlation between MWPI values and proximate measured downburst wind gusts with a confidence level near 100%. Case studies demonstrate the influence of the South Asian monsoon on convective storm environments and the response of the downburst prediction algorithm.

Keywords: severe convective storms, convective windstorms, meteorological geostationary satellites, numerical weather prediction

1. INTRODUCTION

Over the contiguous United States (CONUS), development and application of a convective storm downburst prediction algorithm using meteorological geostationary satellite data has demonstrated success[1, 2] where convective-storm generated wind is the most prevalent of all severe convective weather types (i.e. hail, tornadoes, wind). Convective windstorms are often related to the downburst, defined in general as a strong downdraft that induces an outburst of damaging winds on or near the ground[3, 4]. In addition, the North American monsoon (NA monsoon) is particularly active with respect to convective storm activity. Typically, lower- and mid-tropospheric moisture, originating from the tropical Pacific Ocean, Gulf of California, and Gulf of Mexico, respectively, is transported northward and westward over the United States intermountain region where the afternoon boundary layer is deep, well-mixed and unstable[5]. The migration and placement of a subtropical anticyclone, as well as the evolution of pre-existing convective storm activity over the Gulf of California region, influence the transport of both low and mid-level moisture into the southwestern United States, thereby pre-conditioning the lower troposphere for convective instability and subsequent downburst generation. In contrast to the monsoon evolution over western CONUS, the Indian summer monsoon (ISM) or Southwest Monsoon is governed by the development and placement of a monsoon trough over northern India[6] between the months of April and September. The development of the ISM typically results in persistent west to southwesterly low-level wind flow over most of India south of the Himalayas that promotes convective storm development and heavy rainfall. Similar to the NAM, the placement and juxtaposition of the lower tropospheric monsoon trough and the mid to upper tropospheric subtropical ridge (Tibetan High) influence the vertical profile of temperature, moisture and wind and the resultant favorability for deep convective storm development and downburst generation. Downburst potential products

* Ken.Pryor@noaa.gov; 1 301 683-3575

Remote Sensing of the Atmosphere, Clouds, and Precipitation VI, edited by Eastwood Im, Raj Kumar, Song Yang, Proc. of SPIE Vol. 9876, 987618

derived from current Geostationary Operational Environmental Satellite (GOES) sounder data have been developed and evaluated[1, 2]. This study entails exploration, application, and preliminary validation of algorithms that capitalize on the availability of high-resolution meteorological satellite imager and numerical weather prediction (NWP) model data to extend the predictability of downburst-generated winds over the Indian Peninsula region during both the pre-monsoon and monsoon seasons.

During the month of June 2015, the Southwest Monsoon advanced steadily from the southern to the northwestern states of India. The progression of the monsoon affected the relative strength of convective storm downbursts that occurred over India during June and July 2015. Figure 1 shows the progression of the monsoon in which the onset of the monsoon was slightly delayed over southern India while over two weeks early near the Pakistan border. Rao[6] outlined the normal dates of the onset and withdrawal of the monsoon "as determined from rainfall increase and decrease and other synoptic features". During the summer over India, two meridional circulation systems, the monsoon cell and Hadley cell, interact to result in a stratification of wind, temperature and moisture. Rao[6] also noted that the northwestward progression of the monsoon resulted in a gradual decrease in lower-to-middle tropospheric temperature lapse rates, especially between the 850 and 500 mb levels, over central and northwestern India between April and July, which suggests decreased downdraft instability associated with monsoon-driven convective storms. This condition stands in contrast to the onset of the NAM and associated phenomena such as the Gulf Surge[7] that enhance downdraft instability over the southwestern United States by increasing precipitation loading within convective storms while the boundary layer remains relatively dry, well-mixed and unstable. In August 2014, a Gulf Surge resulted in the development of intense thunderstorms over southern California that produced severe downbursts, heavy rainfall, and flash flooding. In general, over the Indian Peninsula, the onset of the summer monsoon results in weaker downburst activity and other convective storm outflow events.

Accordingly, the Microburst Windspeed Potential Index[1] effectively indicated relative downburst intensity in both pre-monsoon and monsoon environments. The MWPI formula that accounts for both updraft and downdraft instability in microburst generation is defined as

$$\mathrm{MWPI} \equiv (\mathrm{CAPE}/100)+\{\Gamma+ (T-T_d)_{850}-(T-T_d)_{670}\} \quad (1)$$

where Γ is the lapse rate (°K km^{-1}) between the lower boundary level (850 mb) and upper boundary level (670 mb) of a layer of consideration, and the quantity (T–Td) represents the dewpoint depression (°K). "CAPE" represents surface-based convective available potential energy (J kg^{-1}), defined as a measure of instability through the depth of the atmosphere. As a supplement to the MWPI product, a multispectral product[8] has been developed and experimentally implemented to assess downburst potential based on the availability of the split window infrared (IR) channels (31 at 11μm, 32 at 12μm) and water vapor (WV) channel (27 at 6.7 μm) of the United States National Aeronautics and Space Administration (NASA) Aqua satellite Moderate Resolution Imaging Spectroradiometer (MODIS). The three-band microburst risk (MBR) product is based on the following algorithm in which the output brightness temperature difference (BTD) is proportional to microburst potential:

$$\mathrm{MBR\text{-}BTD} \equiv (T_{32} - T_{27}) - (T_{31} - T_{32}) \quad (2)$$

Where the parameter T_n represents the brightness temperature observed in a particular imager band. The relationship between BTD and microburst risk in the product image is based on the following assumptions: (1) A deep, well-mixed convective boundary layer exists in the region of interest; (2) moisture for convective storm development is based in the mid-troposphere and is advected over the region of interest; and (3) the mid- to upper- tropospheric layer of moisture is vertically extensive and would yield precipitation if provided a sufficient forcing mechanism. A validation study over the United States southern Great Plains and intermountain northwestern U.S. revealed a high likelihood of severe downbursts (> force 10* or > 25 m s^{-1}) associated with MBR-BTD values greater than 50.

The traditional usage of the brightness temperature difference (BTD) between GOES infrared channel 3 (WV, 6.5μm) and channel 4 (IR, 11μm) is the monitoring of convective storm intensity by detection of overshooting thunderstorm tops. Rabin et.al.[9] noted observations that have shown positive BTD (> 0°K) can occur when water vapor

*Beaufort Scale

exists above cloud tops in a stably stratified lower stratosphere due forced ascent from overshooting tops. Thus, a BTD greater than zero (0°K) has been used a measure for intensity of overshooting convection[9]. An alternative application of the WV-IR BTD technique was proposed by Pryor[1] based on a conceptual model of a dry-air "notch" that was formulated to represent unsaturated air that intrudes into a convective storm and interacts with convective and stratiform precipitation regions, subsequently providing the energy for intense downdrafts and resulting outflow winds. The presence of a dry-air "notch" on the periphery of a convective storm suggests two processes that may enhance storm outflow. On the local storm scale, direct interaction of unsaturated air with the precipitation core results from wake entrainment as described by Knupp[10]. Knupp[10], through numerical simulations, confirmed that entrainment of dry mid-level air into the downshear flank of a convective storm fostered strong downdraft generation. A saturation mixing point analysis detailed in the Knupp study echoed the finding of Normand[11] that the entrainment of unsaturated air into the downshear flank of a convective storm results in a significant wet bulb potential temperature depression that is proportional to the cooling due to evaporation of precipitation. The negative buoyancy induced by this mid-level cooling forces downdraft initiation and acceleration within a deep, moist convective storm. A more pertinent process for mesoscale convective systems (MCSs), such as squall lines and bow echoes, is the rear-inflow of unsaturated air into the trailing stratiform region that results in strengthening of the cold pool. Smull and Houze[12] and Weisman[13] described the process by which the establishment of an elevated, ascending front-to-rear flow originating from the deep, moist convection, overlying a strong and deep outflow-induced cold pool generates and sustains a strong rear-inflow jet. James and Markowski[14] found that in very unstable (large CAPE) environments, rear inflow of unsaturated air into the stratiform precipitation region resulted in the enhancement of downdrafts and the subsequent increase of cold pool strength. A strong cold pool within an MCS serves to sustain the intensity of the leading deep convection region, thereby maintaining the ability of the MCS to generate strong forward flank downdrafts and resulting outflow on the surface.

Figure 2 shows the GOES WV band (3, at 6.8 μm) weighting function peak, overlying peaks in the GOES-11 split window band (4 and 5, at 11 and 12 μm, respectively) functions at the surface, associated with a classic "inverted V" sounding profile over Boise, Idaho during the evening of 30 August 2008. The merged display of the RAOB and weighting functions indicated that the mid-tropospheric moist layer was vertically extensive and was overlying a dry, convective boundary layer, thus, illustrating favorable environmental conditions for strong convective downdrafts. An MBR-BTD value of 51.9°K was calculated over Boise using brightness temperatures related to the GOES-11 weighting functions and was correlated to a downburst-related wind gust of 24 m s^{-1} (46 kt) recorded at the Idaho National Laboratory about two hours later. In contrast, a merged display of the RAOB and GOES-13 weighting functions over Tampa, Florida, in the rear-inflow region of a linear convective system (or squall line) that tracked over southern Florida during the morning of 16 February 2016, is also shown in Figure 2. The RAOB indicated a steep, near dry-adiabatic temperature lapse rate in the mid-troposphere, between the 300 and 600-mb levels, and a co-located dry-air layer, centered at the 500 mb level, with a mixing ratio near zero. In contrast to the thermodynamic profile over Boise, this mid-tropospheric dry-air layer was overlying a vertically extensive surface-based moist layer, which is a condition typically connected to wet downbursts. The WV band weighting function peak near the 400-mb level and the IR band weighting function peak near the surface is associated with a generally large temperature lapse rate between the 300-mb level and the surface. Thus, the BTD value of -37.15°K observed at 1200 UTC over Tampa can be related to a convectively unstable environment with sufficient mid-level dry air to initiate strong downdrafts as the dry air is intruded into the rear flank of the convective storm line and heavy precipitation core.

As shown later in this paper, the blended use of the MWPI, MBR-BTD, and WV-IR BTD products are effective in the diagnosis and prognosis of downburst wind gust potential. This paper will outline the methodology of a study and evaluation of blended satellite and numerical model downburst prediction applications over the Indian Peninsula region. Case studies of two pre-monsoon convective windstorm events and a study of a downburst event over southern India during the monsoon season will demonstrate the effectiveness of the MWPI product and influence of the Southwest Monsoon on convective wind intensity. Favorable results presented in this paper include a statistically significant positive correlation between MWPI values and proximate measured downburst wind gusts over India.

2. METHODOLOGY

The validation, data analysis, and case study process followed the method outlined in Pryor[1,2] with an emphasis on satellite data sources available over the Indian Peninsula region. For each convective windstorm event documented in

Table 1, MWPI values were calculated with 0 to 3 hour forecasts from 0.25 to 0.5° resolution GFS and 0.25° resolution NGFS model thermodynamic profile data in GRIB2 format. In the case studies, MWPI values were plotted on KALPANA-1 Very High Resolution Radiometer (VHRR) 8-km resolution infrared band imagery and 1-km resolution MODIS visible imagery. MWPI values were color-coded according to thunderstorm wind gust potential magnitude (in knots) as illustrated in the regression chart in Figure 3. Employing forecast datasets from NWP models alleviated the requirement for the calculation of time-lagged correlation between MWPI values and observed measured convective wind gusts. Thus, the focus could be shifted from accuracy of the MWPI calculated at an observation (or analysis) time to the accuracy of the NWP model that generates the MWPI value.

The KALPANA-1 satellite is of special interest as the first dedicated geostationary weather satellite built by the Indian Space Research Organization (ISRO) launched into Geosynchronous Transfer Orbit (GTO) in September 2002 with ISRO's Polar Satellite Launch Vehicle (PSLV-C4). Recent studies[15, 16] have demonstrated the effectiveness of KALPANA-1 Very High Resolution Radiometer (VHRR) data in the large-scale and sub-divisional scale estimation of precipitation as validated against satellite infrared (IR) and microwave data, and surface rain gauge observations. The current study applies VHRR data as a background for the numerical weather prediction (NWP) model-derived MWPI product. KALPANA-1 VHRR water vapor-thermal infrared (WV-IR) band BTD was generated as background imagery for the MWPI product. KALPANA-1 VHRR imagery was selected for this study due to the availability of an Integrated Data Viewer (IDV) HDF-5 file conversion utility provided by ISRO Meteorological and Oceanographic Satellite Data Archival Centre (MOSDAC). Blended MODIS and METEOSAT-7 product images were generated by the Man computer Interactive Data Access System (McIDAS)-V program. METEOSAT-7 Visible and InfraRed Imager (MVIRI) 2.5-km resolution visible imagery and 5-km resolution WV imagery were used for the 1 August 2015 Bangalore downburst case study due to the unavailability of MODIS data.

In addition, three-band MBR-BTD images were generated and overlain with WV-IR, cloud top temperature (CTT), and cloud effective radius (r_e) fields calculated from 1-km resolution MODIS datasets. Cloud (particle) effective radius, proportional to cloud liquid and ice water content, is defined as the area weighted mean radius of cloud particles, including precipitation. The effective radius parameter was determined to be important for this study due to the information that could be provided pertaining to cloud microphysics and dynamics within a convective storm, especially in the absence of Doppler meteorological radar data. Rosenfeld et al.[17] described a technique combining cloud top temperature and effective radius to infer updraft strength and dominant precipitation types within a convective storm, thereby determining storm severity. The authors[17]found a combination of cold CTTs (<240°K) and r_e greater than 30μm was associated with hailstorms while a combination of cold CTTs and smaller r_e (<20μm) was associated with convective storms comprised of a high concentration small ice phase precipitation particles (i.e. graupel, small hail). This technique is applied in the current study to derive a relationship between storm cloud characteristics and downdraft severity in which CTT served as a proxy for glaciation temperature (T_g) and r_e served as a proxy for glaciation effective radius (r_g).

KALPANA-1 image datasets were obtained from MOSDAC (available online at http://www.mosdac.gov.in/). METEOSAT-7 MVIRI datasets were obtained from the European Organization for the Exploitation of Meteorological Satellites (EUMETSAT) Earth Observation Portal (available online at https://eoportal.eumetsat.int/userMgmt/login.faces). NASA MODIS datasets were obtained from the Level 1 and Atmosphere Archive and Distribution System (LAADS, available online at https://ladsweb.nascom.nasa.gov/index.html). GFS and NGFS model datasets were obtained from the NOAA National Operational Model Archive and Distribution System (NOMADS, available online at http://nomads.ncdc.noaa.gov/data.php) and the India National Center for Medium Range Weather Forecasting (NCMRWF) FTP server (ftp://ftp.ncmrwf.gov.in/pub/outgoing/IND_REGION), respectively. Measured downburst-related wind speeds, provided by India Meteorological Department (IMD) storm bulletins, were compared directly to the closest representative MWPI values and wind gust potential was calculated from the regression equation displayed in Figure 3 that was derived for the United States southern Great Plains region. This process allowed for the calculation of a correlation coefficient (r) and mean absolute error (MAE) between MWPI values and observed downburst wind gust speeds and comprised a very important part of the performance evaluation of the MWPI product. The validation dataset (MWPI, measured wind speeds) is presented in Table 1 while Table 2 documents the validation results.

3. CASE STUDIES

3.1 28 April 2015 Northeastern India downbursts

During the late morning and early afternoon 28 April 2015, a thunderstorm complex developed over northeastern India and then tracked southeastward through the Ranchi metropolitan area. At this time, as shown in Figure 4, the summer monsoon circulation was not yet apparent, with 500 mb streamlines revealing the Indian Peninsula under the influence of a broad anticyclone that extended from the northern Arabian Sea eastward across central India and the resultant northwesterly flow dominating northern India. The GFS model thermodynamic profile over Ranchi in Figure 5 exhibits an unstable "inverted V" pattern that is frequently related to downburst-producing thunderstorms. The MWPI product, calculated from 0.25° resolution GFS and NGFS model datasets and displayed in Figures 6 and 8, echoes the pattern of the profile, with values between 30 and 33 in the vicinity of Ranchi that indicated wind gust potential near 23 m s^{-1} (45 kt) in accordance with the regression chart in Figure 3. In addition, as shown in Figure 7, Ranchi was located in a region with high MBR-BTD values approaching 50 (red shading) that signified wind gust potential near 25 m s^{-1} (48 kt). Storm cloud effective radius (r_e) measurements between 10 and 20 μm suggested intense updrafts that likely produced large amounts of small hail and graupel that eventually melted and evaporated during descent toward the surface. The MODIS WV-IR product displays a horizontally extensive area of cold cloud tops along the leading edge of the MCS, also revealing the prominence of strong updrafts. Figure 6 shows that both GFS and NGFS model-derived MWPI values, calculated for a valid time of 0900 UTC 28 April 2015 over the Ranchi vicinity, ranged from 25 to 30 and corresponded to wind gust potential of 20 to 23 m s^{-1} (40 to 45 kt). Figure 8, the GFS model three-hour forecast MWPI, valid at 0900 UTC, shows a local maximum (30 to 33) immediately downstream of the southeastward-moving MCS while a prominent dry-air notch and WV-IR BTD maximum (5° K) became apparent on the rear (northwestern) flank of the MCS by 0845 UTC. At 0850 UTC, a downburst wind gust of 24 m s^{-1} (47 kt) was recorded at the IMD observatory at Ranchi Birsa Munda Airport (VERC).

3.2 13 June 2015 New Delhi downbursts

By the middle of June 2015, the Southwest Monsoon had progressed northward, with the leading edge extending from Gujarat to West Bengal, and a dry air mass with northwesterly flow was still in place over northern India, as shown in Figure 9. During the afternoon 13 June 2015, a thunderstorm complex developed over northern India and then tracked southeastward through the New Delhi metropolitan area. The strongest measured thunderstorm winds, most likely associated with a downburst, occurred near a local maximum in MWPI values that corresponded with the "inverted V" thermodynamic profile shown in Figure 10. Blended KALPANA-1 VHRR WV – IR BTD, MODIS, and GFS/NGFS model MWPI product images shown in Figures 11 and 13 effectively signify downburst potential with this thunderstorm complex. Figure 11, a comparison between the MWPI product calculated from 0.5° resolution GFS model and 0.25° resolution NGFS model data, valid at 0900 UTC, exhibits comparable performance with values near 30 indicating wind gust potential of 20 to 23 m s^{-1} (40 to 45 kt) based on the regression chart shown in Figure 3. In addition, the MBR-BTD product shown in Figure 12, in a similar manner to the BTD product for the 28 April case, reveals MBR-BTD values approaching 50 (red shading) in the New Delhi area that correlate to wind gust potential of 23 to 26 m s^{-1} (45 to 50 kt). Figure 12 also shows a comparison between the MODIS WV-IR BTD, CTT and effective radius (r_e) product images about 90 minutes prior to the occurrence of severe thunderstorm winds in the New Delhi area. Effective radius measured between 25 and 35 μm in the forward flank of the MCS and lower WV-IR BTD values (1° K) corresponded to slightly weaker storm updrafts as compared to the updraft strength inferred for the 28 April case, but, indicated a larger liquid and ice water content possibly associated with the presence of larger hail. Although no hail was observed at the surface in the New Delhi area associated with this storm, the METAR observation at Indira Gandhi International Airport in Figure 11 suggests that loading due to heavy rainfall was likely a factor in downburst generation. Figure 13 shows the evolution of the thunderstorm complex that tracked over New Delhi into a "bowing" pattern, with a local maximum in MWPI values immediately downstream of the MCS. Between 0920 and 1000 UTC, thunderstorm wind gusts of 23 m s^{-1} (45 kt) and 16 m s^{-1} (31 kt) were recorded by IMD observatories at Safdarjung Airport and Indira Gandhi International Airport, respectively. Overall, the combined wind gust prediction derived from GFS/NGFS model data and MODIS data of 20 to 26 m s^{-1}(40 to 50 kt) was verified by the convective wind gust measured at Safdarjung Airport observatory.

3.3 1 August 2015 Bangalore downburst

During the afternoon of 1 August 2015, the summer monsoon trough was well-established over northern India, as shown in Figure 14, and resulted in lower tropospheric westerly flow over the southern Indian Peninsula. Clusters of thunderstorms developed over the coastal region and the Western Ghats of Karnataka and then tracked east and southeastward as illustrated in blended METEOSAT-7 and KALPANA-1 MWPI product images in Figures 15 and 16. MWPI values between 15 and 18, calculated from 0.5° resolution GFS model and 0.25° resolution NGFS model data, valid at 1200 UTC over the south-central Indian Peninsula indicated wind gust potential of 18 to 20 m s^{-1} (35 to 40 kt) in accordance with the regression chart in Figure 3. Figure 17 exhibits the monsoon circulation over Bangalore in the NGFS model vertical wind profile as a transition from westerly flow to easterly flow above the 400 mb level. The vertical juxtaposition of moist easterly upper-tropospheric flow over downslope westerly flow from the Western Ghats, and afternoon surface heating resulted in the development of a convective mixed layer and the shallow "inverted V" thermodynamic profile shown in Figure 17. By early evening, near 1305 UTC, a thunderstorm that developed along an outflow boundary produced a strong downburst, with a wind gust of 18 m s^{-1} (34 kt) recorded at Bangalore International Airport (white triangle). With a value of 15 immediately downstream of Bangalore, that correlated to wind gust potential of 19 m s^{-1} (38 kt), the higher-resolution NGFS MWPI product was slightly more accurate, as presented in the comparison in Figure 15. An Aqua satellite pass was not available over this region during the early evening of 1 August, and thus, MBR-BTD and r_e were not calculated for this case study.

4. DISCUSSION AND CONCLUSIONS

Validation results for the 2015 season are favorable, with a positive correlation between MWPI values and proximate measured downburst wind gusts as documented in Table 2. The correlation coefficient (r) for 22 downburst events from April to August 2015 was computed to be near 0.6 with a confidence level near 100% for both the GFS and NGFS model MWPI products. The high confidence level, in which the computed t values were higher than the critical value for 21 data samples (3.8), underscores the likelihood of the correlation resulting from chance coincidence is near 0%. Table 1 documents the 22 downburst events that were recorded between April and August 2015. The tendency of the MWPI to overestimate wind gust potential based on a regression equation derived for the United States Great Plains suggests that the regression relationship needs to be modified for downbursts that occur over India. The NGFS-derived MWPI exhibited a slightly lower MAE (+5.5 kt) and a higher critical value (6.46) as compared to the statistics for the GFS MWPI, and, thus, demonstrated more effective forecasting ability over the Indian Peninsula region. Although the lower MAE associated with the NGFS MWPI suggests a higher accuracy, this value actually results from the averaging of larger errors, especially for MWPI values calculated in more humid regions of southern and northeastern India (i.e. Bangalore, Kolkata). The larger errors likely result from precipitation phase and storm forward motion effects as discussed in Pryor[2].

Figures 5, 10, and 17 show the thermodynamic profiles associated with each downburst event described in the case studies. Note that the downburst occurrences were associated with varying degrees of the "inverted V" thermodynamic profile as displayed in skew-T-log p diagrams, and that the stronger downburst activity in the Ranchi and New Delhi areas was associated with a more pronounced "inverted V" profile representing the generally drier pre-monsoon environment over northern India. The stronger convective wind gust observed at Ranchi, as compared to winds measured in the New Delhi area on 13 June, could be attributed to a higher concentration of smaller ice-phase precipitation particles, especially graupel and small hail. Srivastava[18] found that a particle size distribution consisting of a high concentration of smaller particles, both ice and liquid, further enhances downdraft intensity and noted that in the case of two storms with similar precipitation content, the storm with a higher concentration of smaller particles will produce a stronger downdraft. The weaker downburst occurrence observed at Bangalore on 1 August, during the monsoon season, was associated with a thermodynamic profile characterized by a deep moist layer that extended from near the surface to the mid-troposphere and a larger vertical distance between the level of free convection (LFC) and the freezing level (FRZL) that likely resulted in a storm that was dominated by liquid phase precipitation. The profile comparison highlights the importance of a well-mixed, unsaturated sub-cloud layer in the generation of downdraft energy and consequent downdraft acceleration. A comparison of maximum WV-IR BTD values in Figures 8, 13, and 16, for each downburst-producing storm in the case studies, exhibits a relative decrease in wind gust intensity with decreasing BTD, and suggests that the storms with higher ice-phase precipitation content are capable of producing stronger downbursts.

Important future work on the development of downburst prediction applications over India will consist of further product validation to obtain a larger sample size that should increase the strength of the correlation between MWPI values and observed downburst wind gust speeds. Pryor[1,2] noted that a sample size of 50 or greater, consisting of paired MWPI values and associated downburst wind observations, is necessary to establish a robust statistical relationship. IMD Doppler radar data, especially reflectivity and differential reflectivity, and application of the MWPI to INSAT-3D and hyperspectral sounder profile datasets, especially Aqua Atmospheric Infrared Sounder (AIRS) and NOAA Unique CrIS/ATMS Processing System (NUCAPS) can be used to cross-validate and inter-compare with NGFS model data. Finally, more exploration of the influence of ISM intensity on general convective storm activity and resultant downburst magnitude is necessary. Prasad and Hayashi[19] discussed patterns of summer monsoon intra-seasonal variability including the influence of weak and "break" episodes on convective storm and rainfall intensity. Inter-comparison of the MWPI to monsoon intensity parameters such as the Horizontal Wind Shear Index[19] (HWSI) may provide more insight into the relationship between the occurrence severe convective winds and circulation patterns associated with different phases of the Indian summer monsoon.

ACKNOWLEDGEMENTS

The author thanks V. S. Prasad and C. J. Johny of the National Center for Medium Range Weather Forecasting for providing the NGFS model datasets used in this research effort. The author also thanks Ghansham Sangar and Shivani Shah of the Space Applications Centre (ISRO) for providing the IDV utility to visualize KALPANA-1 datasets.

REFERENCES

[1] Pryor, K. L., "Downburst prediction applications of meteorological geostationary satellites," Proc. SPIE 9259, 925910 (2014).
[2] Pryor, K. L., "Progress and Developments of Downburst Prediction Applications of GOES," Wea. Forecasting 30(5), 1182–1200 (2015).
[3] Fujita, T. T., [The Downburst, Microburst and Macroburst], University of Chicago, Chicago, 1-18, (1985).
[4] Wakimoto, R. M., "Forecasting dry microburst activity over the high plains," Mon. Wea. Rev. 113(7), 1131-1143 (1985).
[5] Adams, D. K. and Comrie, A. C., "The North American Monsoon," Bull. Amer. Meteor. Soc. 78(10), 2197–2213 (1997).
[6] Rao, Y. P., [Southwest Monsoon], India Meteorological Department, New Delhi, 2-5 (1976).
[7] Hales, J. E., "Surges of maritime tropical air northward over the Gulf of California," Mon. Wea. Rev. 100(4), 298–306 (1972).
[8] Pryor, K. L., "Microburst windspeed potential assessment: progress and developments," Proc. 16th Conf. on Satellite Meteorology and Oceanography, JP6.12 (2009).
[9] Rabin, R., Bothwell, P., and Weiss, S., "Temperature deviation from equilibrium temperature: convective overshoot from satellite imagery," http://overshoot.nssl.noaa.gov (2016).
[10] Knupp, K. R., "Numerical simulation of low-level downdraft initiation within precipitating cumulonimbi: Some preliminary results," Mon. Wea. Rev. 117(7), 1517-1529 (1989).
[11] Normand, C. W. B., "Energy in the atmosphere," Quart. J. Roy. Meteor. Soc. 72(312), 145-167 (1946).
[12] Smull, B. F., and Houze, Jr., R. A., "Rear inflow in squall lines with trailing stratiform precipitation," Mon. Wea. Rev. 115(12), 2869-2889 (1987).
[13] Weisman, M. L., "The role of convectively generated rear inflow jets in the evolution of long-lived mesoconvective systems," J. Atmos. Sci. 49(19), 1826–1847 (1992).
[14] James, R. P., and Markowski, P. M., "A numerical investigation of the effects of dry air aloft on deep convection," Mon. Wea. Rev., 138(1), 140–161 (2010).
[15] Prakash, S., Mahesh, C., and Gairola, R. M., "Large-scale precipitation estimation using Kalpana-1 IR measurements and its validation using GPCP and GPCC data," Theor, Appl. Climatol., 106 (3), 283-293 (2011).
[16] Mahesh, C., Prakash, S., Gairola, R. M., Shah, S., and Pal, P. K., "Meteorological sub-divisional scale rainfall monitoring using Kalpana-1 VHRR measurements," Geographical Research, 52(3), 328-336 (2014).

[17] Rosenfeld, D., Woodley, W. L., Lerner, A., Kelman, G., and Lindsey, D. T., "Satellite detection of severe convective storms by their retrieved vertical profiles of cloud particle effective radius and thermodynamic phase," Journal of Geophysical Research: Atmospheres, 113(D4), D04208 (2008).
[18] Srivastava, R.C., "A model of intense downdrafts driven by the melting and evaporation of precipitation ," J. Atmos. Sci. 44(13), 1752–1773 (1987).
[19] Prasad, V.S., and Hayashi, T., "Active, weak and break spells in the Indian summer monsoon," Meteorol. Atmos. Phys. 95(1), 53-61 (2007).

TABLES AND FIGURES

Table 1. A list of downburst events with measured wind speeds compared to GFS and NGFS model-derived MWPI values for the 2015 pre-monsoon and monsoon seasons.

Date	Time (UTC)	Measured Wind Speed (kt)	Measured Wind Location	GFS MWPI	NGFS MWPI
3-Apr	1620	31	Jodhpur (VIJO)	13	15
	1730	27	Jaipur (VIJP)	14	12
4-Apr	1458	31	Guwahati (VEGT)	12	9
5-Apr	1045	31	Silchar (VEKU)	22	19
13-Apr	1030	25	Bengaluru (VOBL)	14	14
17-Apr	1239	44	Gaya (VEGY)	24	20
21-Apr	1330	38	Kolkata (VECC)	49	47
	1343	58	Kolkata (Doppler)	49	47
22-Apr	1536	35	Kolkata (VECC)	54	41
23-Apr	1237	57	Bengaluru (VOBG)	28	22
25-Apr	1204	34	Bengaluru (VOBG)	25	18
28-Apr	850	47	Ranchi (VERC)	30	25
	1250	28	Alipore (VEBA)	15	19
2-May	1645	27	Guwahati (VEGT)	7	0
	1655	32	Alipore (VEBA)	33	22
3-May	916	32	Bankura	22	23
13-Jun	920	45	New Delhi (VIDD)	30	30
	1000	31	New Delhi (VIDP)	30	30
14-Jun	1345	27	Bengaluru (VOBG)	15	9
6-Jul	1830	22	New Delhi (VIDP)	9	13
9-Jul	1249	31	Bengaluru (VOBL)	17	12
1-Aug	1306	34	Bengaluru (VOBL)	18	15

Table 2. MWPI validation statistics based on direct comparison between index values and measured downburst wind gusts.

	GFS MWPI (N=22)	NGFS MWPI (N=22)
MEA (kt)	+6.5	+5.5
Correlation (r)	0.61	0.59
t value	4.79	6.46
Critical Value (P< 0.0005)	3.82	3.82

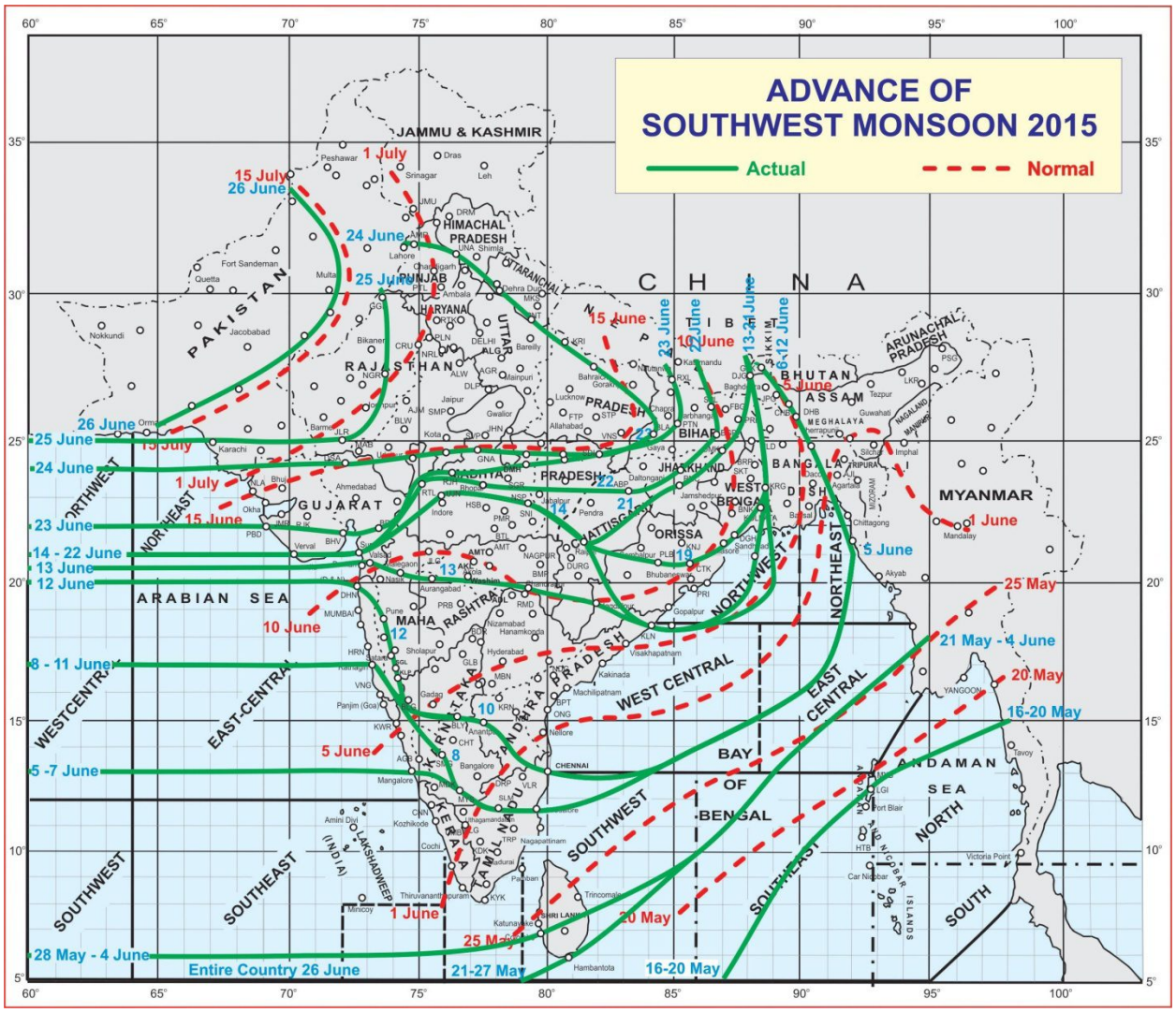

Figure 1. Progression of the Southwest Monsoon over India during May and June 2015. Courtesy of the India Meteorological Department (available online at http://www.imd.gov.in/section/nhac/dynamic/Monsoon_frame.htm).

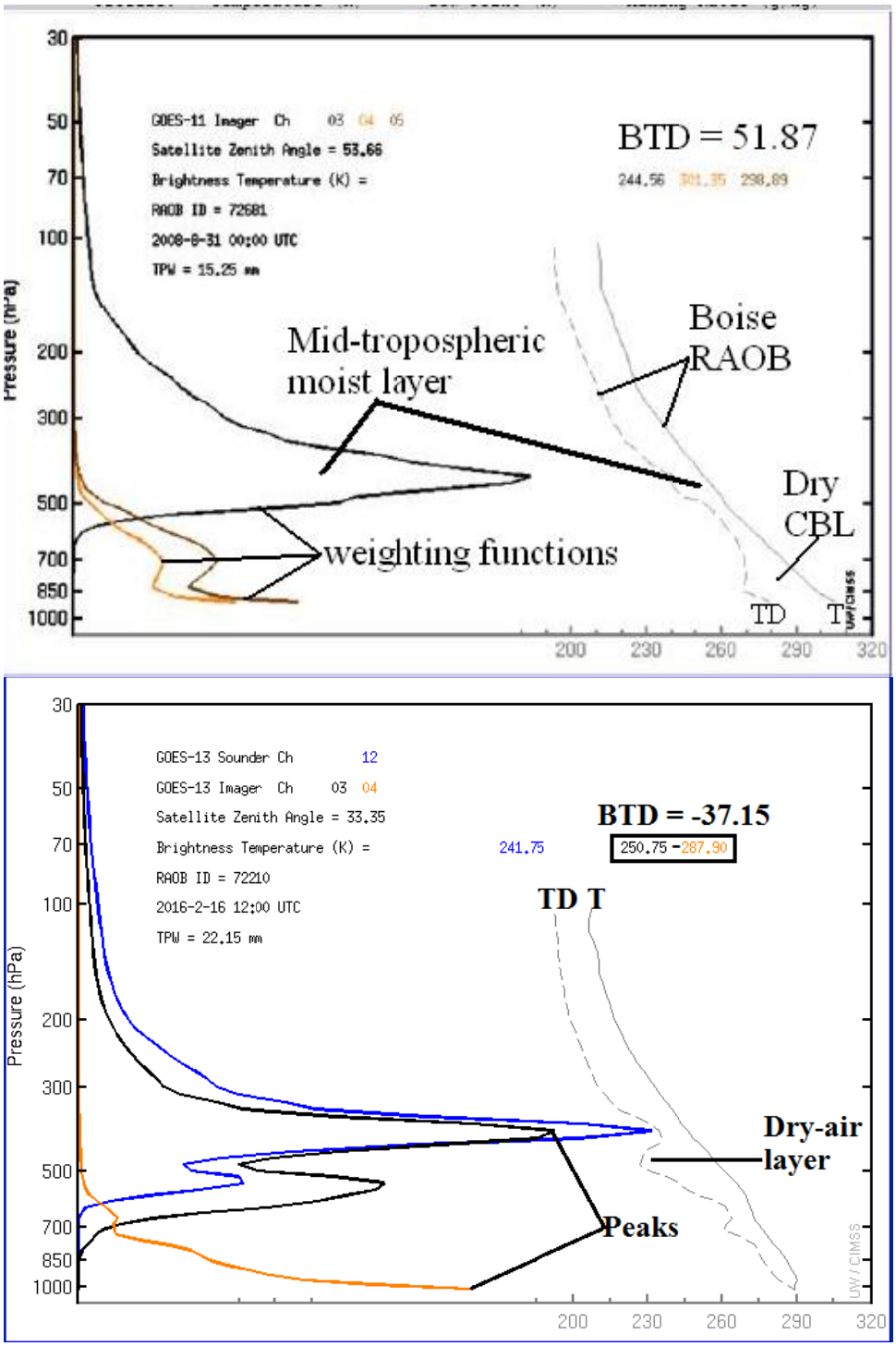

Figure 2. GOES-11 imager transmittance weighting functions for bands 3 (WV, 6.8 μm), 4 (IR, 11μm, and 5 (IR, 12 μm) compared to the radiosonde observation (RAOB) profile over Boise, Idaho at 0000 UTC 31 August 2008 (top); GOES-13 imager transmittance weighting functions for bands 3 and 4 compared to the RAOB profile over Tampa, Florida at 1200 UTC 16 February 2016 (bottom) with temperature (T) and dewpoint (TD) curves displayed.

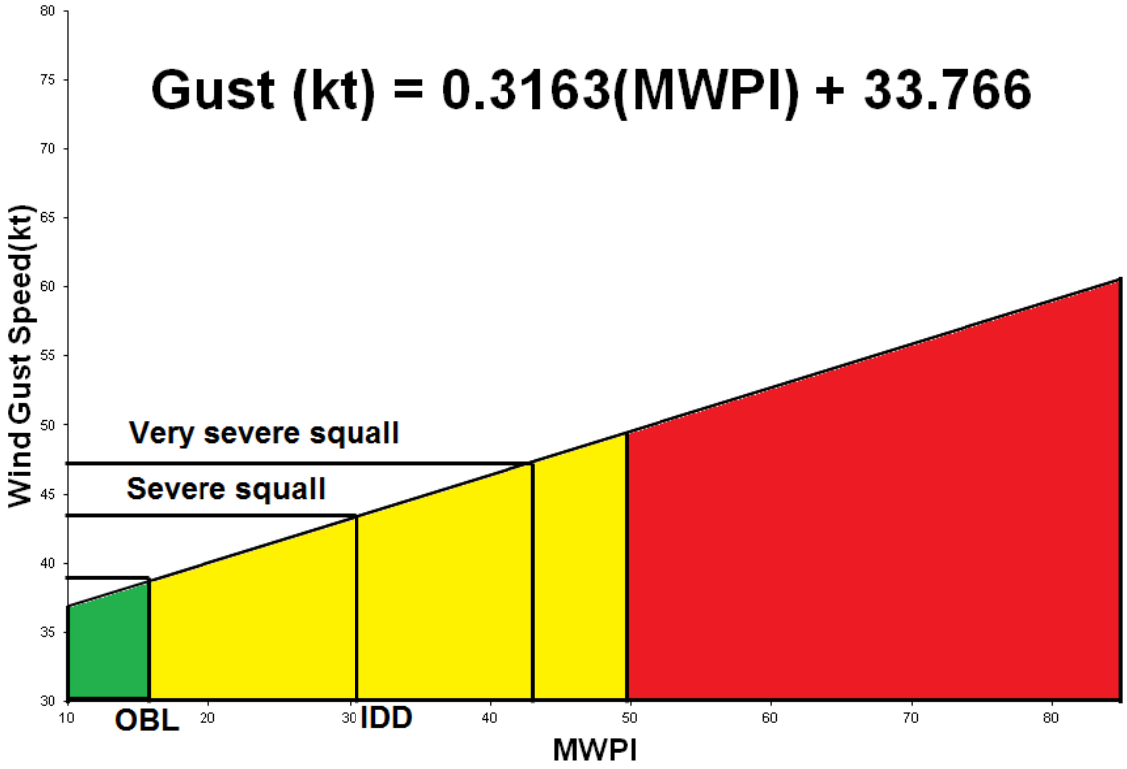

Figure 3. Regression chart based on a linear regression equation derived from 208 downburst wind events that occurred over the United States Great Plains region between 2007 and 2010. Wind gust predictions for downburst events at Bangalore (OBL) and New Delhi (IDD) are indicated on the chart.

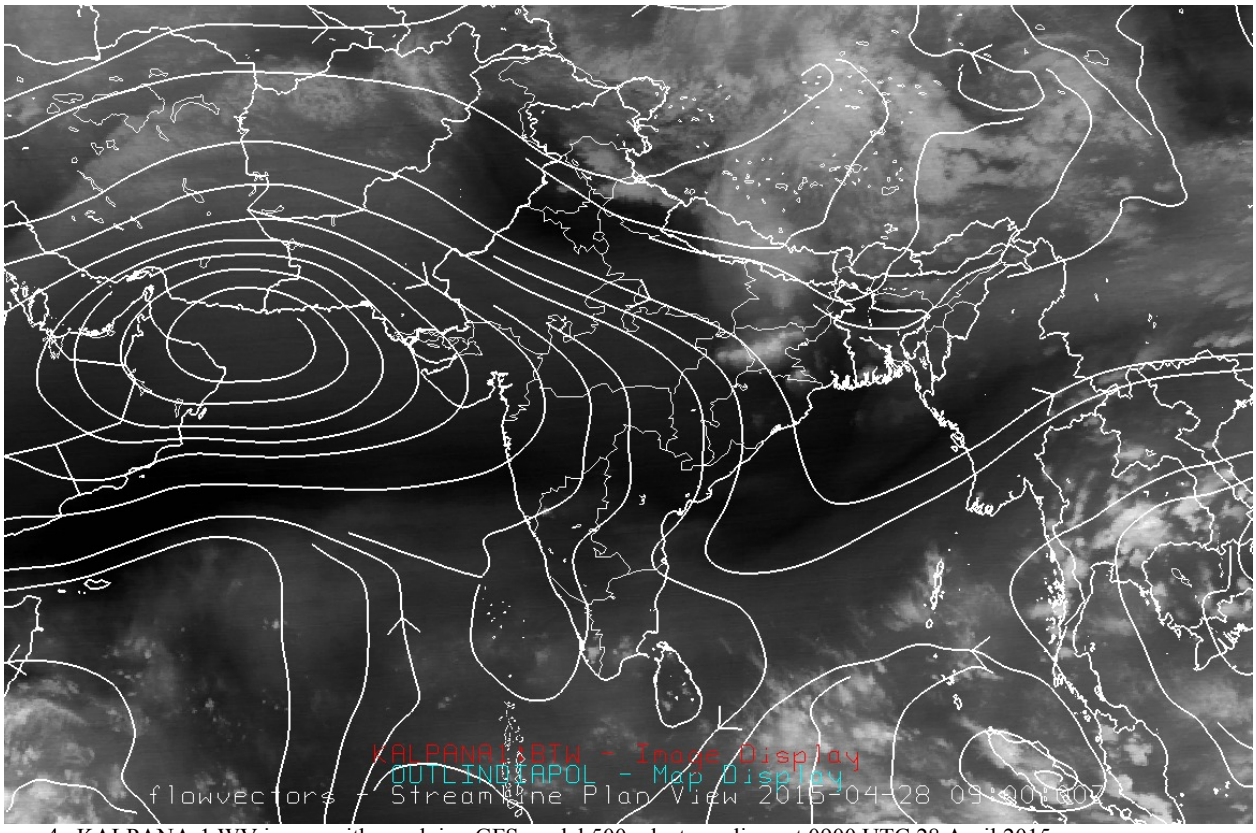

Figure 4. KALPANA-1 WV image with overlying GFS model 500 mb streamlines at 0900 UTC 28 April 2015.

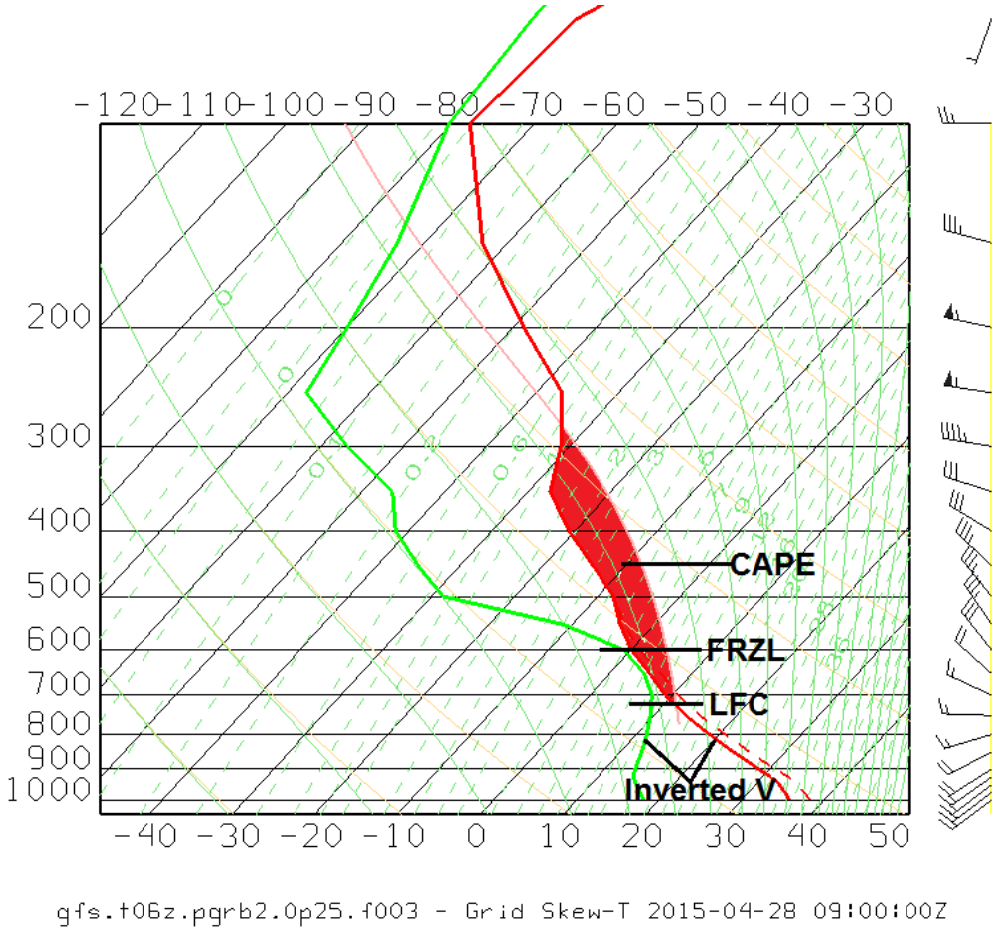

Figure 5. GFS model thermodynamic profile over Ranchi, India valid at 0900 UTC 28 April 2015. Red-shaded area represents CAPE. "FRZL" represents the freezing level and "LFC" represents the level of free convection.

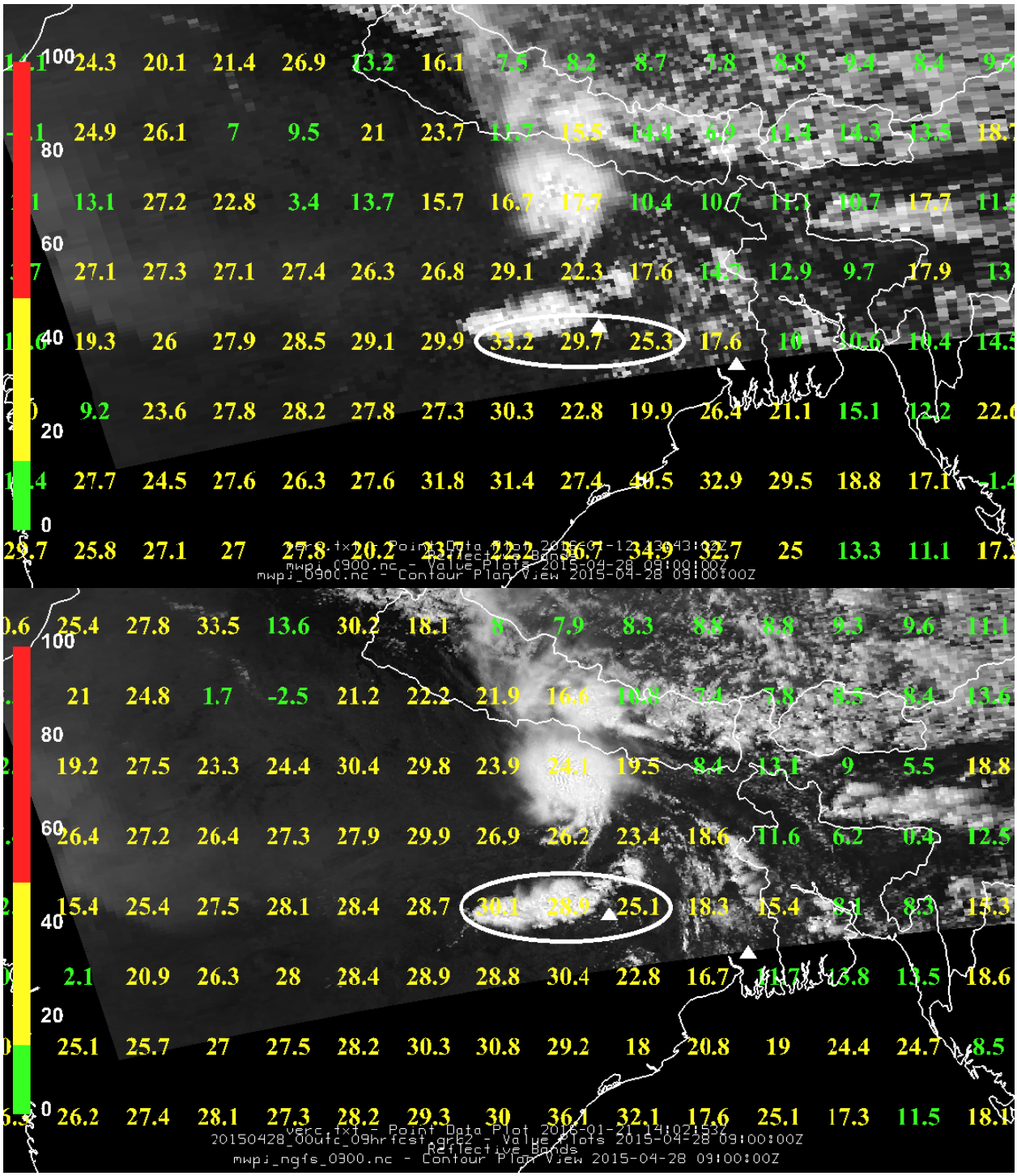

Figure 6. GFS MWPI (top) compared to NGFS MWPI (bottom) valid at 0900 UTC plotted over MODIS visible imagery at 0740 UTC 28 April 2015. White-outlined region marks the location of the inter-comparison between the NGFS and GFS versions of the MWPI. White triangle near the center of the image marks the location of Ranchi, India.

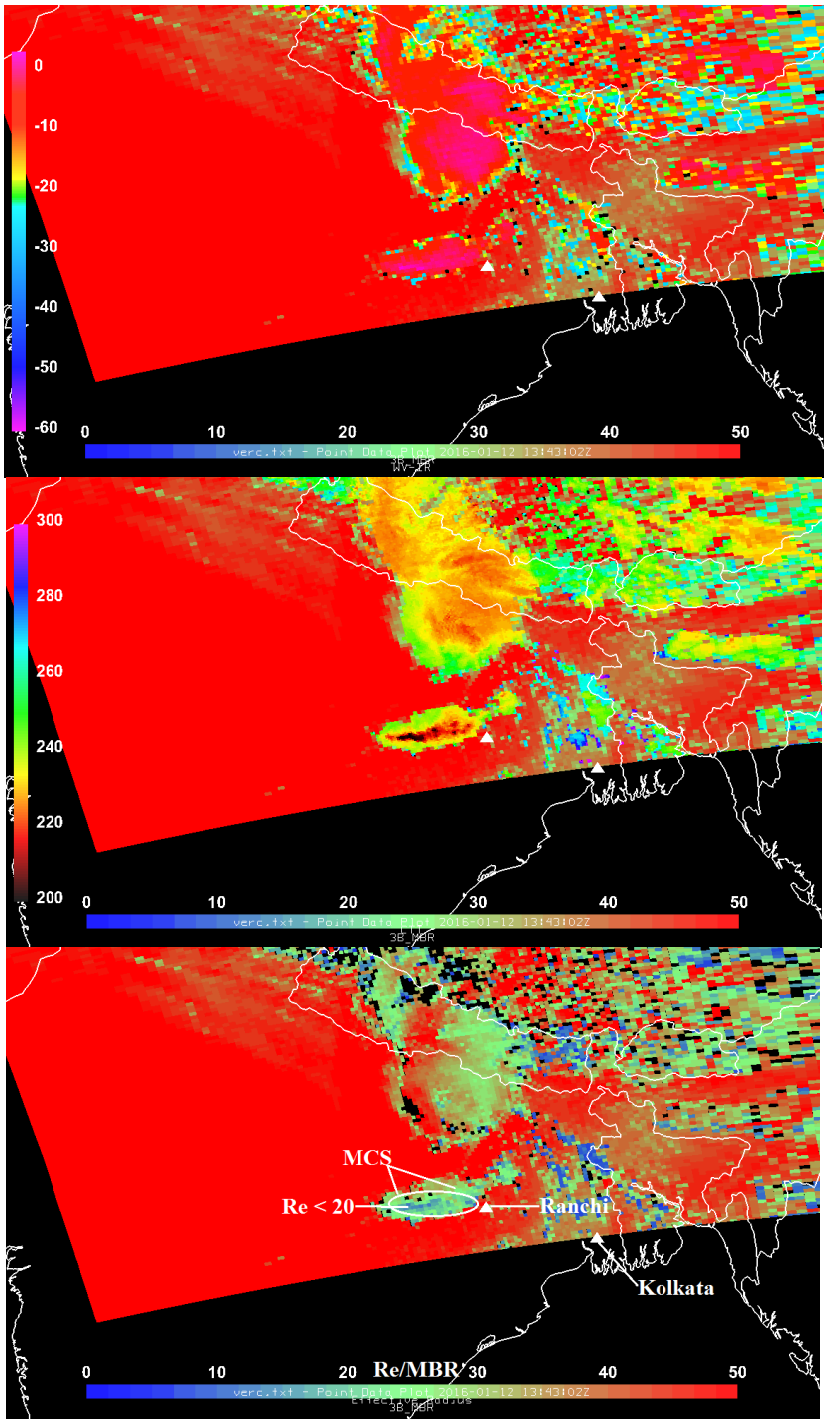

Figure 7. MODIS blended WV-IR BTD and three-band MBR product image at 0740 UTC 28 April 2015 (top). Color bars for WV-IR and MBR are shown on the left side and bottom of the BTD image, respectively. MODIS blended Cloud Top Temperature (CTT, middle), Cloud Effective Radius (R_e, bottom) and MBR product images at 0740 UTC 28 April 2015 with color bars for CTT, R_e, and MBR on the sides of the images. White triangle near the center of the image marks the location of Ranchi, India.

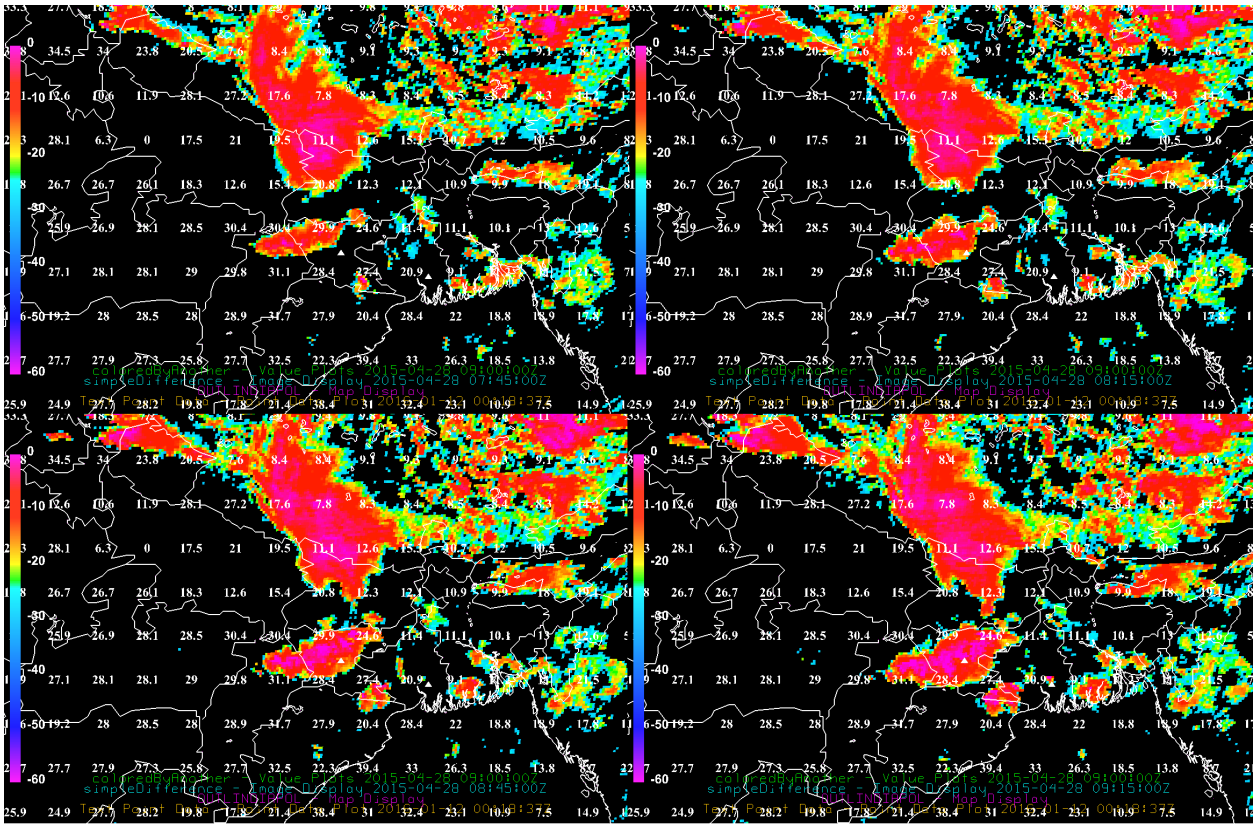

Figure 8. GFS MWPI valid at 0900 UTC 28 April 2015 plotted over KALPANA-1 WV-IR BTD product imagery at 0745 UTC (top left), 0815 UTC (top right), 0845 UTC (bottom left), and 0915 UTC (bottom right) 28 April 2015. BTD color bar is displayed on the left side of the images. The closest maximum WV-IR BTD to Ranchi at 0845 UTC was 5° K.

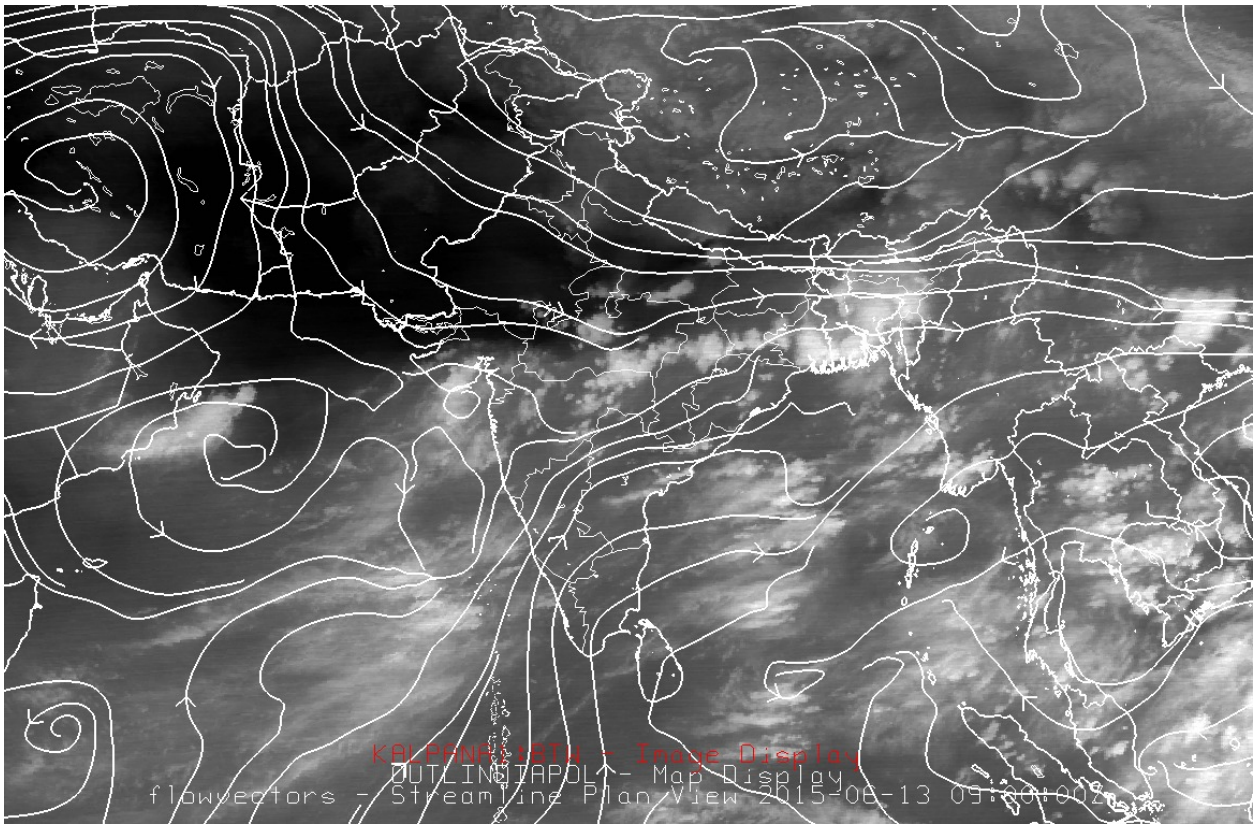

Figure 9. KALPANA-1 WV image with overlying GFS model 500 mb streamlines at 0900 UTC 13 June 2015.

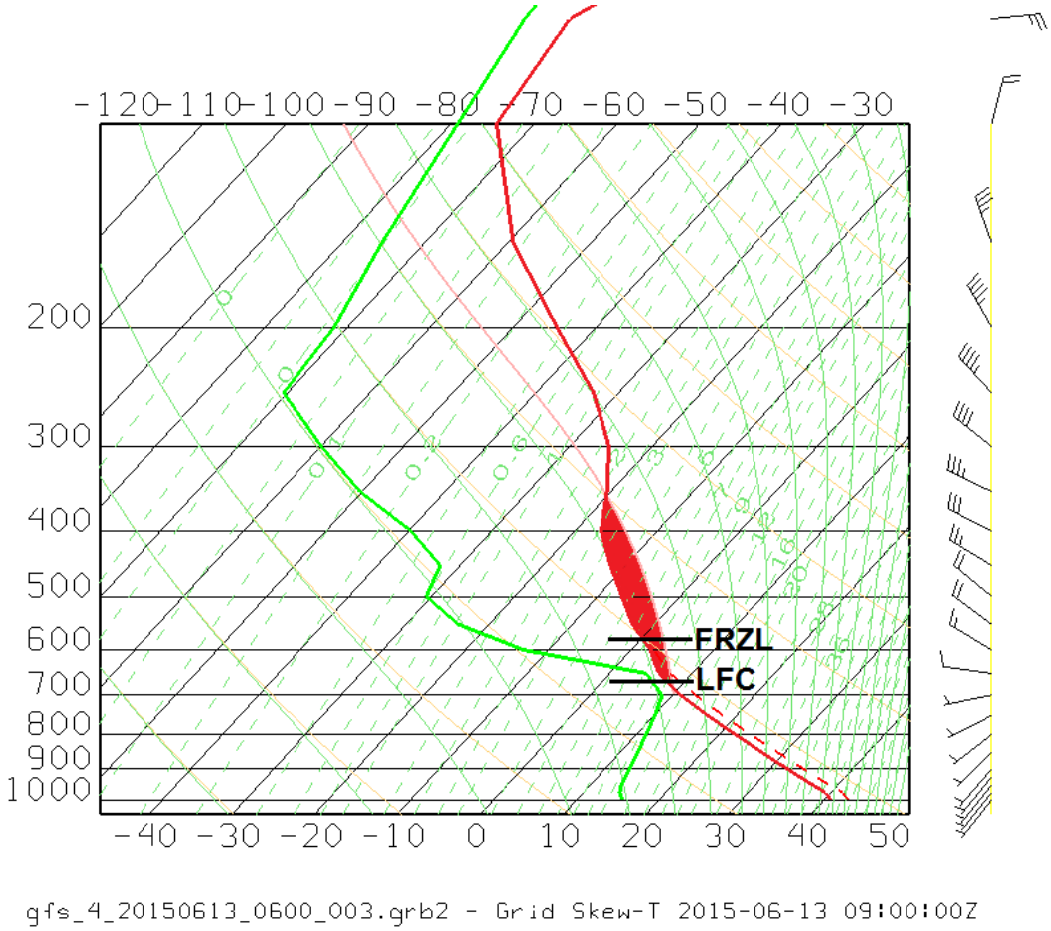

Figure 10. GFS model thermodynamic profile over New Delhi, India valid at 0900 UTC 13 June 2015. Red-shaded area represents CAPE. "FRZL" represents the freezing level and "LFC" represents the level of free convection.

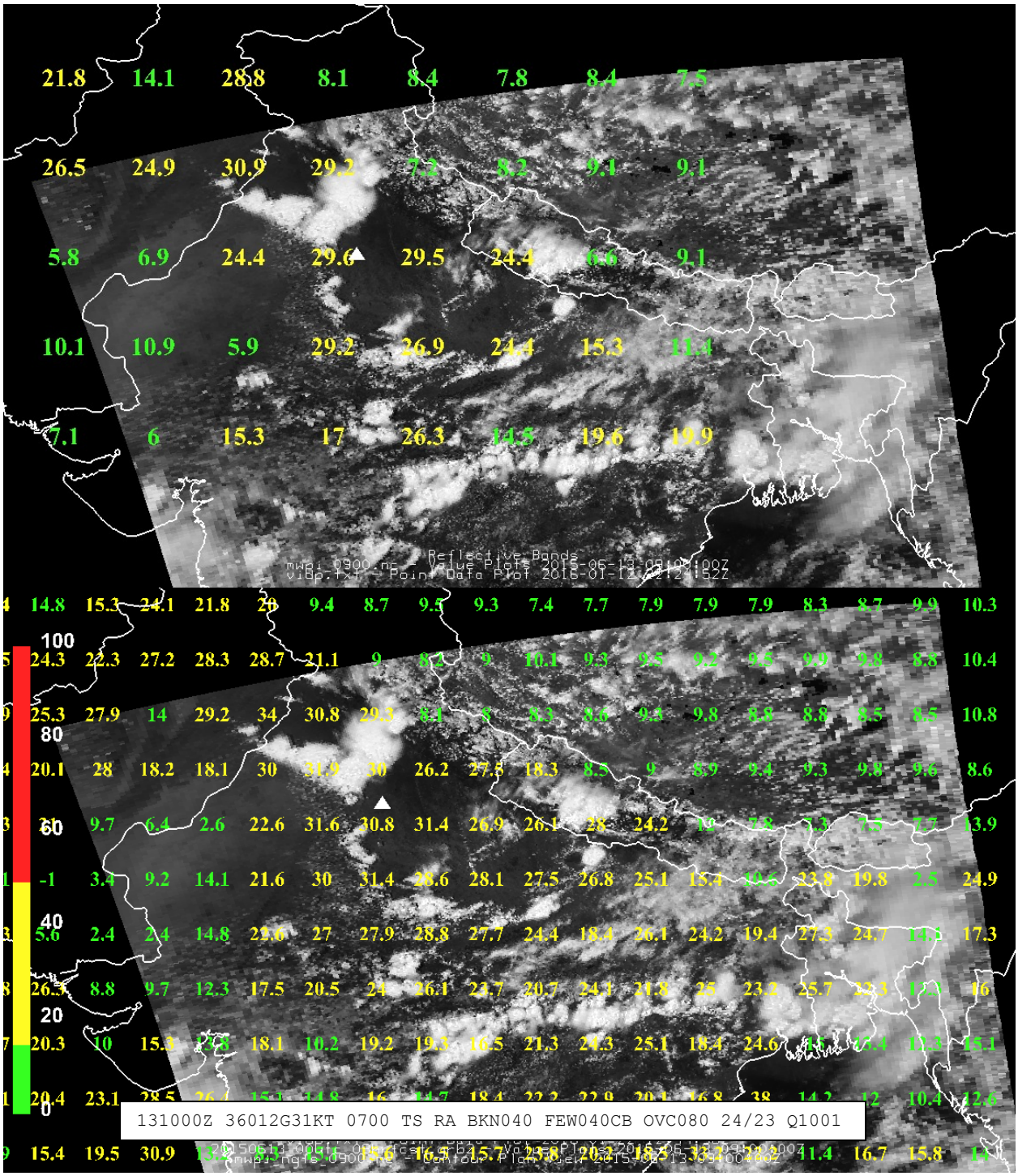

Figure 11. Comparison of GFS MWPI (top) to NGFS MWPI (bottom) valid at 0900 UTC plotted over MODIS visible imagery at 0750 UTC 13 June 2015. METAR observation at Indira Gandhi International Airport is displayed at the bottom of the NGFS MWPI product image. White triangle near the center of the image marks the location of New Delhi, India.

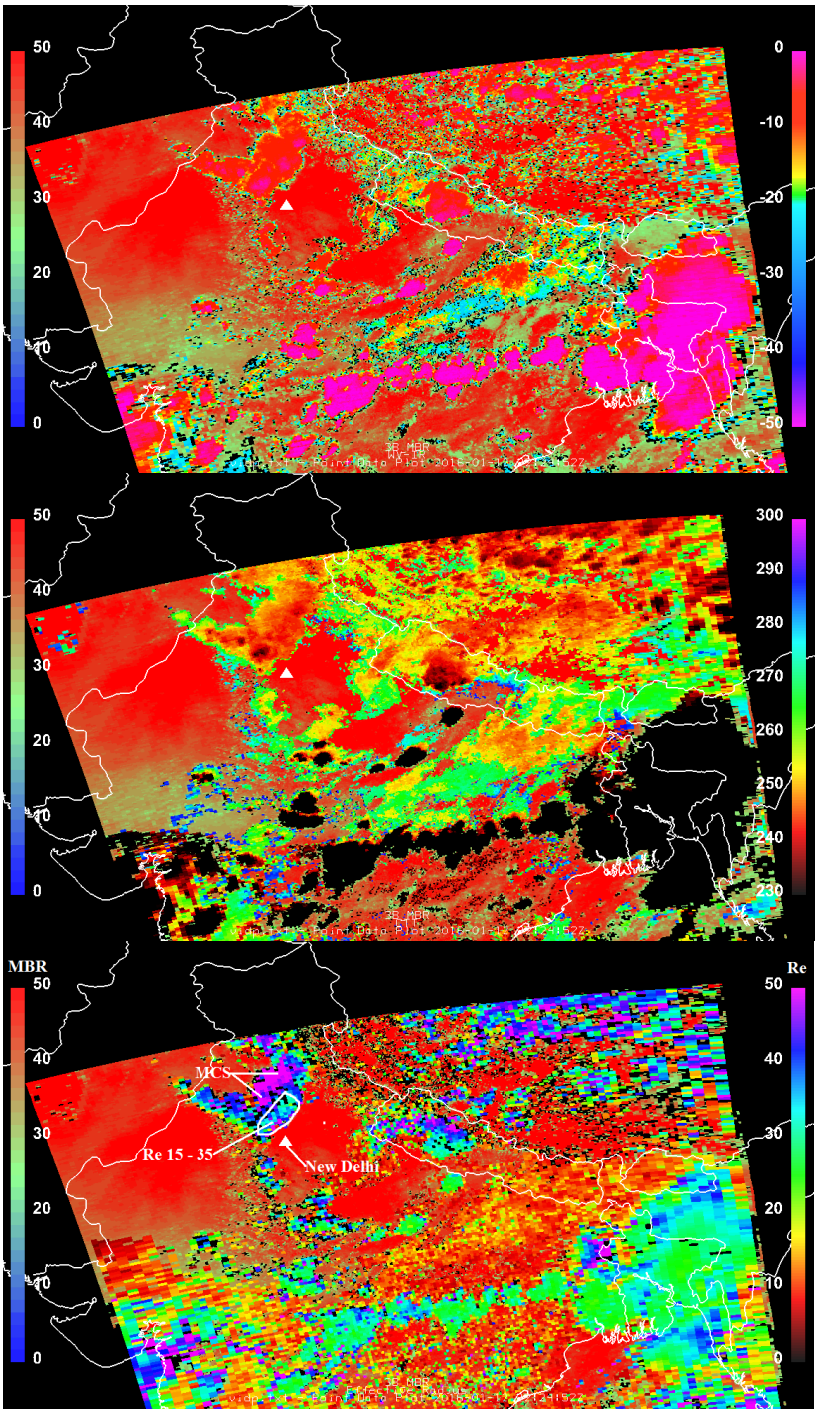

Figure 12. MODIS blended WV-IR BTD and three-band MBR product image at 0750 UTC 13 June 2015 (top). Color bars for MBR and WV-IR are shown on the left and right sides of the BTD image, respectively. MODIS blended Cloud Top Temperature (CTT, middle), Cloud Effective Radius (R_e, bottom) and MBR product images at 0750 UTC 13 June 2015 with color bars for CTT, R_e, and MBR on the sides of the images. White triangle near the center of the image marks the location of New Delhi, India.

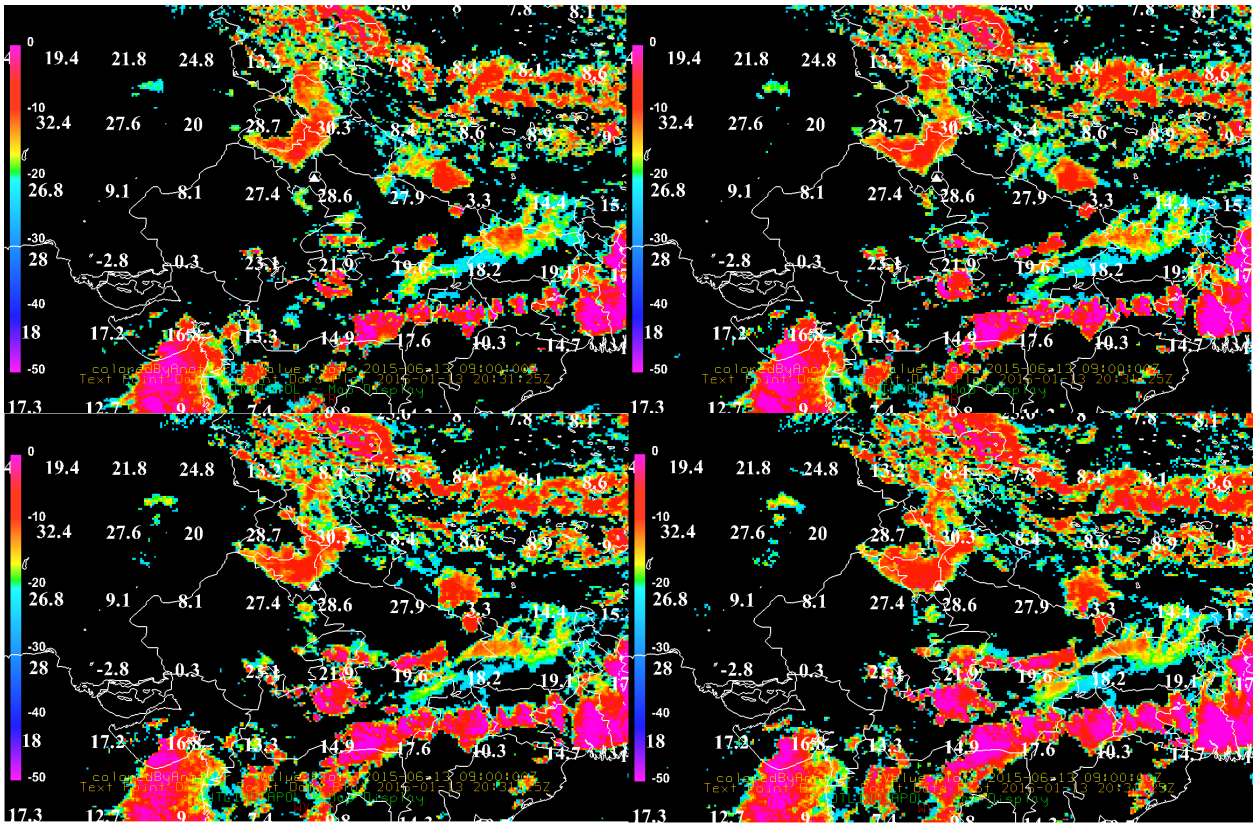

Figure 13. GFS MWPI valid at 0900 UTC 13 June 2015 plotted over KALPANA-1 WV-IR BTD product imagery at 0745 UTC (top left), 0815 UTC (top right), 0845 UTC (bottom left), and 0915 UTC (bottom right) 13 June 2015. BTD color bar is displayed on the left side of the images. The closest maximum WV-IR BTD to New Delhi at 0915 UTC was 1° K.

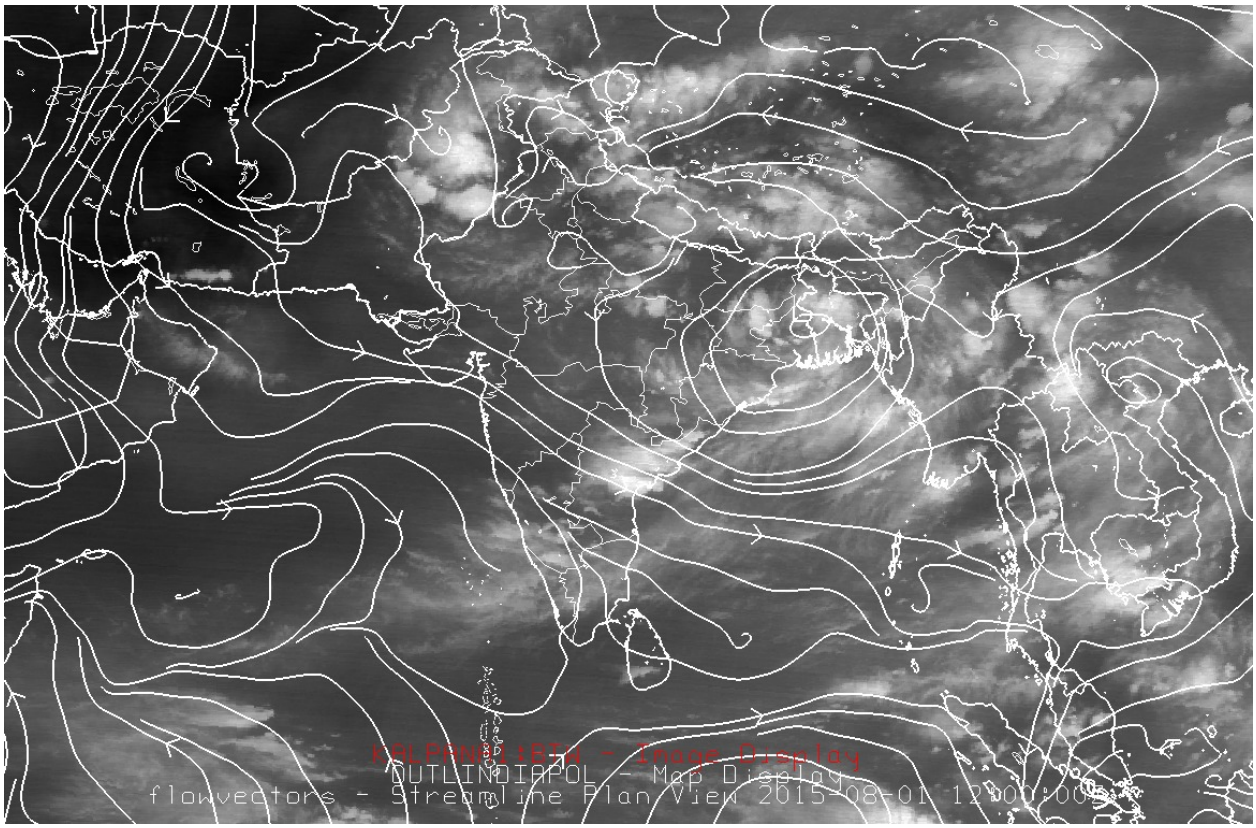

Figure 14. KALPANA-1 WV image with overlying GFS model 500 mb streamlines at 1200 UTC 1 August 2015.

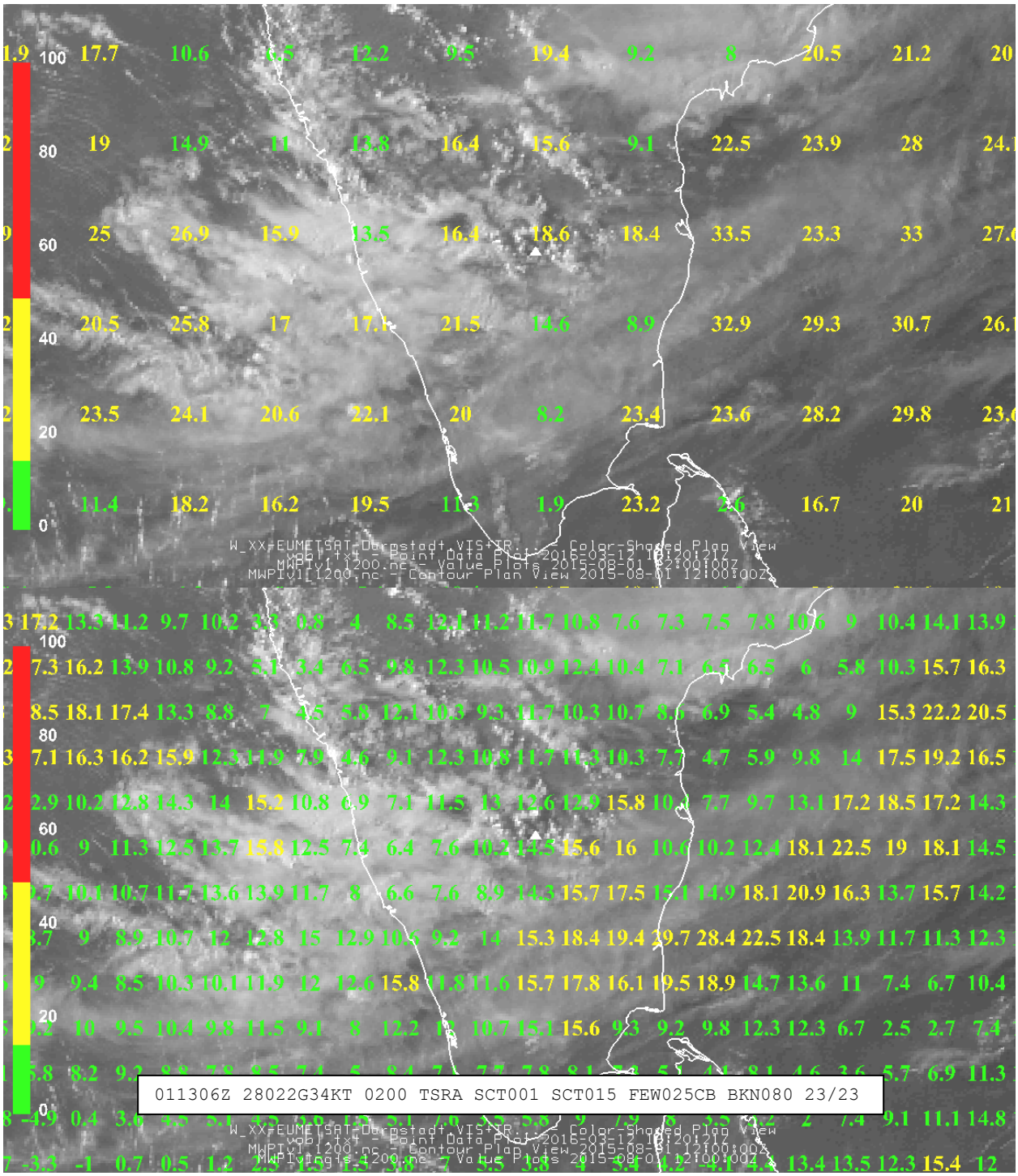

Figure 15. Comparison of GFS MWPI (top) to NGFS MWPI (bottom) overlying METEOSAT-7 VIS image at 1200 UTC 1 August 2015. White triangle marks the location of Bangalore, India. METAR observation at Bangalore International Airport is displayed at the bottom of the NGFS MWPI product image.

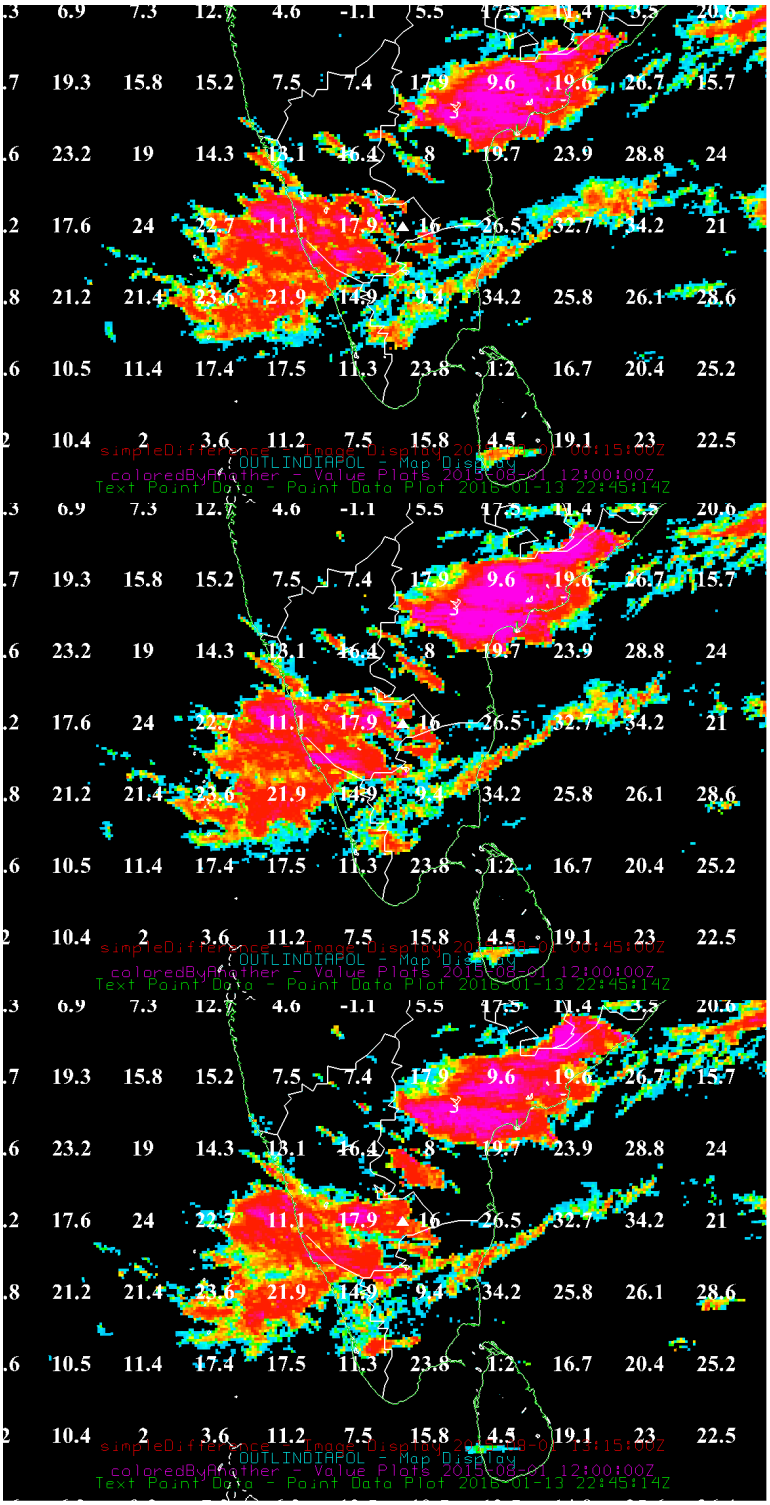

Figure 16. GFS MWPI valid at 1200 UTC 1 August 2015 plotted over KALPANA-1 WV-IR BTD product imagery at 1215 UTC (top), 1245 UTC (middle), and 1315 UTC (bottom), 1 August 2015. The closest maximum WV-IR BTD to Bangalore at 1315 UTC was -2° K.

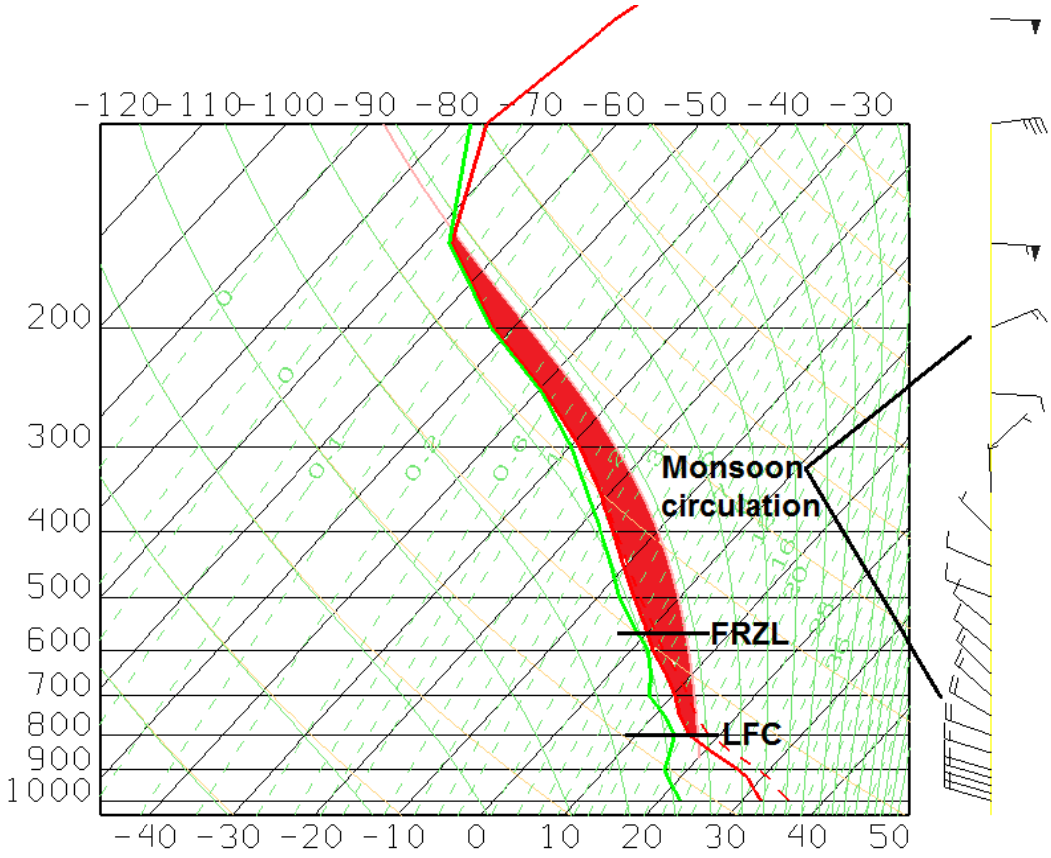

Figure 17. NGFS model thermodynamic profile over Bangalore valid at 1200 UTC 1 August 2015. Red-shaded area represents CAPE. “FRZL” represents the freezing level and “LFC” represents the level of free convection.